Physicochemical and electrochemical characterization of Nafion-type membranes with embedded silica nanoparticles: Effect of functionalization

M.V. Porozhnyy, S.A. Shkirskaya, D.Yu. Butylskii, V.V. Dotsenko, E.Yu. Safronova, A.B. Yaroslavtsev, S. Deabate, P. Huguet, V.V. Nikonenko

Physicochemical and electrochemical characterization of Nafion-type membranes with embedded silica nanoparticles: effect of functionalization

M.V. Porozhnyy[1], S.A. Shkirskaya[1], D.Yu. Butylskii[1], V.V. Dotsenko[1,2], E.Yu. Safronova[3], A.B. Yaroslavtsev[3], S. Deabate[4], P. Huguet[4], V.V. Nikonenko[1]

[1]*Kuban State University, 149 Stavropolskaya Street, Krasnodar 350040, Russian Federation*

[2]*North Caucasus Federal University, 1a Pushkina street, Stavropol 355009, Russian Federation*

[3]*N.S. Kurnakov Institute of General and Inorganic Chemistry, Russian Academy of Sciences, 31 Leninsky Prospekt, 119991, Moscow, Russian Federation*

[4]*IEM (Institut Européen des Membranes), UMR 5635 (CNRS-ENSCM-UM), Université Montpellier, Place E. Bataillon, F-34095, Montpellier, France*

Abstract

Introduction of nanoparticles in membranes allows a significant enhancement of their performance in energy production, water treatment and other applications. However, the effect of nanoparticles' surface functionalization and the mechanism of their impact on membrane properties remain poorly studied. In this paper, we examine a Nafion-based membrane and its modifications, each containing 3 wt% SiO_2. The effect of functionalization by propyl, 3-aminopropyl and 3,3,3-trifluoropropyl is investigated. The water uptake, contact angle, conductivity, diffusion permeability to NaCl, current-voltage curves (CVC), chronopotentiograms (ChP), and the difference between the pH of the desalination compartment output and input solutions (characterizing the water splitting rate) are reported. It is found that the doping of the membranes with nanoparticles leads to increasing their conductivity in all cases except 3-aminopropyl, which imparts a positive charge to the nanoparticles; the diffusion permeability decreases and permselectivity increases in all cases. The latter is explained by transformation of the mesoporous membrane structure to the microporous one. The impact of nanoparticles on the membrane conductivity, CVC and ChP is mainly caused by an additional (positive) space charge introduced into the pore solution and at the membrane surface by the electric double layer surrounding the nanoparticles. The greater the surface charge density of the nanoparticles and the smaller their size, the stronger the impact. Accordingly, the highest conductivity, current density at a low fixed voltage and chronopotentiometric transition time are shown by the sample doped with SiO_2 and 3,3,3-trifluoropropyl. The interplay between electroconvection and water splitting phenomena is discussed.

Keywords: *ion-exchange membrane; silica nanoparticles; electrochemical properties; microheterogeneous.*

1. Introduction

In the context of global environmental concerns (global warming, air and water pollution, waste disposal, etc.), membrane technologies are receiving increasing attention. Indeed, various applications of these technologies can essentially contribute to the solution to many ecological problems and, thus, ensure sustainable development.

Despite a large range of commercially available membranes [1], there is a great scientific interest in improving membrane properties via their modification, especially when the modification is aimed at the improvement of a specific characteristic. One of the most promising methods is the immobilization of inorganic nanoparticles in polymer membranes. The hybrid organic-inorganic membranes obtained in this way show a better performance in a number of applications [2–4]. For example, proton exchange membranes doped with metal oxide particles can have higher water uptake and conductivity at elevated temperatures and low relative humidity, which is important in fuel cell applications [5–9]. However, the modification of Nafion membranes with SiO_2 and TiO_2, while improving water retention, does not always lead to increasing conductivity [6,10,11]. Better conductivity is detected, when the inserted particles exhibit acidic properties [10,12,13]. It is also found that water uptake and conductivity of hybrid materials increase, when some hydrophilic functional groups are grafted to incorporated silica particles [14]. This type of functionalization of nanoparticles can results also in increasing ion-exchange capacity (IEC) of the membrane [15,16].

Membrane modification with nanoparticles is very important not only for a better performance of fuel cells, but also for separation processes in different industries [17]. Indeed, this modification along with increasing membrane conductivity allows reducing diffusion permeability and improving membrane permselectivity [18] and ion-exchange selectivity [19]. The introduction of oxide particles in the membranes for gas separation and pervaporation processes makes it possible to improve permeability, selectivity, and thermal stability of these membranes [4,20]. Embedding metal oxide particles (sometimes grafted) in ultrafiltration and osmosis membranes leads to an increase in their hydraulic permeability and fouling resistance when using them in wastewater desalination and treatment processes [21,22]. Hybrid ion-exchange membranes (IEMs) were proposed and successfully implied as the redox flow batteries separators [23] and in other applications [24] for their improved selectivity and conductance properties. The interactions of nanoparticles with cell membranes have a very high importance for biomedical applications such as drug delivery and anti-cancer treatments [25–28].

Although there are many studies on the properties of natural and artificial membranes with nanoparticles, the mechanism of their effect on the membrane global characteristics remain unclear. Some authors [29] make accent on increasing ion exchange capacity and consider the introduction of inorganic nanoparticles in polymer IEMs as a promising method of producing membranes with high IEC without compromising mechanical strength. However, in many cases, the IEM performance was found enhanced after the incorporation of nanoparticles, although there was no noticeable increase in IEC [11,30]. It is known that the size and surface charge density of nanoparticles seem to be the main properties, which determine the impact of nanoparticles [31]. There are a number of publications modelling the space charge and electric double layer (EDL) around nanoparticles in aqueous solutions [32–35]. However, there are only a few publications devoted to the mathematical description of the ion transport in IEMs doped with nanoparticles [36,37] in particular with the attempt to quantitively relate the parameters of nanoparticles (their size and surface charge density) with electrochemical characteristics (conductivity, permselectivity) [38]. A similar situation takes place concerning the effect of functionalization. Although this effect is rather well studied for the nanoparticles in aqueous solutions, in particular, in the case of silica nanoparticles [39], there are rare publications about the relationship between the nature of reagent for functionalizing nanoparticles and the resulting membrane properties. Generally, only one or two membrane properties, subject to the action of the functionalization, are considered. Thus, Berbar et al. [19] try to find such a functionalization of silica nanoparticles incorporated in SPES membranes, which maximizes the elimination and the separation of Pb^{2+} and Cd^{2+} ions present in a feed aqueous solution. The effect of functionalization on the Nafion-type membrane conductivity (in pure water, the membrane in the H^+ form) and permeability regarding NaCl and HCl diffusion is studied in Refs. [36,40]. It was found that the membrane conductivity of the modified membranes was generally higher and the diffusion permeability lower than in the case of non-modified membranes. In particular, a high conductivity was found in the case of non-functionalized silica and a low diffusion permeability in the case of silica functionalized with perfluorododecyl groups [40]. This trend is explained by the model of the membrane limited elasticity [4]: hydrophilic groups of nanoparticles attract water, which results in increasing size of pores and conducting channels. The impact of the space charge in the pore solution created by the nanoparticles is also important [38,41]; this space charge replaces the electroneutral solution situated in the center of pores, thus increasing conductivity and reduces diffusion of electrolyte.

However, the impact of nanoparticles on the membrane properties is not sufficiently understood. Although generally the importance of the nanoparticle surface charge density for the membrane conductivity and diffusion permeability was recognized [38], and the effect of nanoparticles on effective ion diffusion coefficients was established [36,42], there are no

publications where the effect of nanoparticles on the current-voltage curves (CVC), chronopotentiograms (ChP) and other electrochemical characteristics would be studied. In addition, too little is known about how functionalization of nanoparticles affects the membrane electrochemical characteristics and how it is connected with the change in the membrane structure. In this paper, we present a comprehensive electrochemical investigation of a series of Nafion-type membranes doped with silica nanoparticles whose surface is functionalized by different reagents. For the first time, we investigate the impact of nanoparticles' functionalization on the membrane electrochemical and physicochemical characteristics and are trying to find a correlation between different electrochemical characteristics, some of which are related to the properties of the membrane volume (for example, conductivity), and others, to the surface (e.g. CVC). The main attention is paid to the nanoparticle surface charge density, its role in the interaction of nanoparticles with the membrane matrix, and the influence on the mechanism of transfer phenomena.

2. Materials

A series of Nafion-based membranes modified with functionalized SiO_2 nanoparticles were prepared via casting procedure developed earlier [40]. One sample was obtained by casting from a Nafion solution containing tetraethoxysilane (TEOS) as a precursor. The precursor was hydrolyzed within the membrane matrix. Three other samples were prepared using the same solution (Nafion + TEOS) containing additionally different silane coupling agents resulting in the formation of different functional groups (Table 1) bonded to the surface of the SiO_2 nanoparticles. The Nafion solution with the precursor and functionalizing agent (if any) was cast onto the Petri dish. After solvent evaporation, the samples were pressed and put in an ammonium-water solution needed for the formation of nanoparticles by hydrolysis and condensation reactions. These composite membranes have the same mass fraction of the nanoparticles (3 wt%), the composition and properties of the nanoparticle core are the same. However, the surface properties of the nanoparticles vary from sample to sample due to different functional groups (Table 1).

Table 1. Studied membranes and some characteristics

Sample		Contact angle, degree	Water uptake, W_u, $g_{H2O}/g_{dry\ mb}$, %	f_{2app}
I	Nafion	66±3	22±1	0.13±0.02
II	Nafion + 3 wt% SiO_2	70±3	23±1	0.11±0.02
III	Nafion + 3 wt% SiO_2 (5 mol% 3-aminopropyl)	57±3	23±1	0.06±0.01

IV	Nafion + 3 wt% SiO_2 (5 mol% propyl)	70±3	24±1	0.05±0.01
V	Nafion + 3 wt% SiO_2 (5 mol% 3,3,3-trifluoropropyl)	68±3	22±1	0.04±0.01

Sample I is a solution-cast Nafion® membrane. Sample II is a modification of the solution-cast Nafion® membrane by non-functionalized silica nanoparticles. Due to the interactions with water, silanol functional groups (-Si-O-H) are present on the surface of the nanoparticle (Fig. 1) [43]. Sample III contains silica nanoparticles functionalized by 3-aminopropyl moieties (5 mol% of $–(CH_2)_3$-NH_2 in relation to the Si atoms). The bonded compound bears an amino group on the end (Fig. 2). Sample IV includes silica nanoparticles functionalized by propyl groups, which are nonpolar and rather hydrophobic. Sample V contains nanoparticles with grafted weak polar hydrophobic 3,3,3-trifluoropropyl groups (Fig. 2).

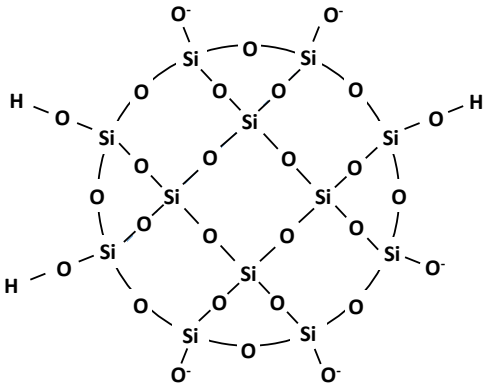

Fig. 1. Schematic structure of a silica nanoparticle with partially ionized silanol functional groups on the surface.

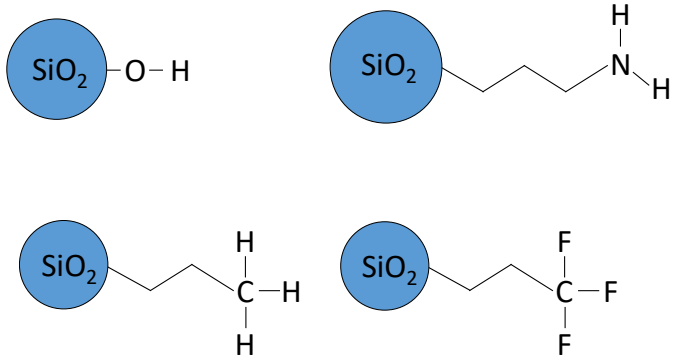

Fig. 2. Schematic representation of nanoparticle body (circles) and grafted functional groups. The radius of the nanoparticles is not to scale with the chain length of the functional groups.

The size of nanoparticles was determined by the images obtained by transmission electron microscopy (TEM). In the case of sample II, this size was in the range 3-7 nm (Fig. 3). The results of the nanoparticles' distribution on the membrane surface and cross-section obtained using a Carl Zeiss NVision 40 scanning electron microscope with an energy-dispersive X-ray (EDX) analysis are presented in the Supplementary materials. These results show the dopant particles are presented both on the surface and in the bulk of the modified membranes.

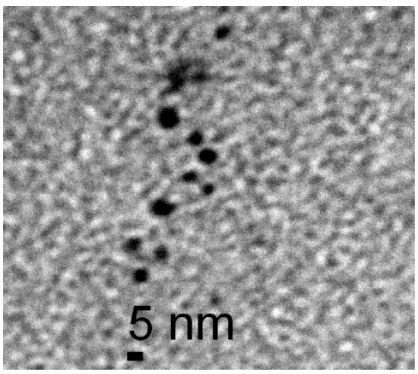

Fig. 3. TEM image of a Nafion-type membrane with 3 wt% silica nanoparticles synthesized in situ (sample II).

3. Experimental

The membrane conductivity, diffusion permeability, IEC, water uptake, contact angles were measured as well as the current-voltage characteristics, chronopotentiograms and change in pH of the solution after passing through the desalination compartment of the ED cell.

The concentration dependence of membrane conductivity is measured by the mercury-contact method where the membrane conductivity is found from the membrane resistance measured as an active portion of membrane impedance using the cell described in [44]. The measurements are conducted in NaCl solutions with different (from 10^{-3} to 0.2 M) concentrations.

The measurements of the concentration dependence of diffusion permeability are carried out in the range of 0.01 to 1M NaCl using a two-compartment cell [45].

The water contact angle was measured using the sessile drop technique according to the procedure described in [46]. The test liquid was distilled water. The contact angles were registered 20 s after the application of a test drop.

The water uptake (W_u) was found as: $W_u\% = \frac{(W_1 - W_2)}{W_2}\ 100$. The wet weight of the sample (W_1) was determined after soaking the membrane in distilled water and rapid wiping of the surface with a filter paper. The dry weight (W_2) was found after drying the sample at 100 °C to constant weight. The data for contract angle and water uptake are shown in Table 1.

To find the IEC, the membranes were converted initially in H^+ form by soaking them in a 1M HCl solution. Then, after careful rinsing in deionized water, membranes were immersed in a 0.1M KCl solution (pH=6) to replace H^+ ions by K^+. The concentration of the released H^+ ions was determined using the potentiometric titration with NaOH. The IEC value was calculated as follows: $\mathrm{IEC} = \frac{V_{NaOH} \times C_{NaOH}}{W_2}$. Note that only part of the H^+ ions attached to the functional groups was replaced by K^+ ions. Another part remained bound to the protonated groups according to the

exchange equilibria at pH=6. In this way we obtain the IEC referred to pH=6, at which all the experiments were performed, and not the total IEC, which is generally higher.

The results of above measurements show (Table 1) that the value of IEC is the same for all the samples within the experimental error (5%) and equal to 0.9 mmol cm^{-3} of swollen membrane. Similarly, the water uptake is nearly the same (23±2 g H_2O/g dry mb) for all the samples. As well, the contact angle does not change significantly after the modification, except for sample III, the surface of which is slightly more hydrophilic than that of the others.

The experimental setup for measuring current-voltage characteristics and chronopotentiograms consists of a laboratory electrodialysis (ED) cell with hydraulic and measuring systems (Fig. 1s, see Supplementary materials). The pH and conductivity values were controlled just before entering and after leaving the desalination compartment of the ED cell. The limiting current density was calculated using the Lévêque equation [47], when knowing the NaCl diffusion coefficient and concentration at the entrance of the desalination compartment (c=0.02 mol L^{-1}) not changing during the experiment; the velocity of the solution flow between the membranes forming the desalination compartment (V_0=0.36 cm s^{-1}), the intermembrane distance (h=0.63 cm) and the membrane active area length (L=2 cm). The counterion effective transport number in the cation-exchange membrane under study (T_1) was taken equal to 1 taking into account that the feed solution was diluted. For the above conditions, the limiting current density calculated using the Lévêque equation, was i_{lim}= 1.97 mA cm^{-1}. The details of the measurements are described in the Supplementary materials.

4. Results and discussion

4.1. Characteristics of nanoparticles

Since the properties of nanoparticles depend also on the porous structure of the host membrane, note that sample I (the sample without nanoparticles) is more porous than commercial Nafion membranes. This difference is due to the preparation method describe above. The water uptake is only slightly higher than that of Nafion® 117 (20 wt% according to Saarinen et al. [48]). However, there is another parameter, denoted f_{2app}, which is more sensitive to changes in membrane structure. This parameter roughly characterizes the volume fraction of electroneutral solution in the membrane. If the structure is microporous (the pore size < 2 nm), there is no electroneutral solution in the membrane, f_{2app}=0. In the case of conventionally homogeneous IEMs [49], which contain micro- and mesopores, f_{2app} is in the range 0.05−0.13. In heterogeneous IEMs, there are also macropores, and f_{2app} is in the range 0.13−0.3. More information about the meaning of f_{2app} is in Section 4.2.2.

The value of f_{2app} is significantly higher for sample I (0.13) than for Nafion® 117. For the latter, f_{2app} is from 0.05 to 0.012 depending on the conditioning procedure, as reported by Berezina et al. [50], and 0.065 according to Chaabane et al. [51], who used a standard conditioning. This relatively large porosity correlates with the values of the counterion transport number, which are essentially lower (Section 4.2.3) than those for the commercial Nafion membranes.

Sample II contains non-functionalized silica nanoparticles with silanol functional groups (-Si-O-H) on their surface (Fig. 1) [4]. These groups are acidic, they become negatively charged when they are ionized and release H^+ into the surrounding solution. Sonnefeld et al. [32] found from electrokinetic experiments that the space charge density of a silica nanoparticle, σ, in NaCl solutions is between −0.01 and −0.025 C m^{-2}, when the NaCl concentration is in the range from 10^{-3} M to 10^{-1} M and pH=6; the absolute value of σ increases with increasing the electrolyte concentration. At 0.01 M NaCl and pH=6, σ≈ −0.02 C m^{-2} [32], which is created by the SiO^- sites located on the surface in the amount of 0.125 sites per nm^2; that is, about 3% of sites on a SiO_2 nanoparticle are negatively charged. The charge density of the nanoparticle is about 5 times lower than that of the pore wall. The latter for a Nafion membrane whose exchange capacity is 1 mol L^{-1} of swollen membrane, can be evaluated as −0.11 C m^{-2} or 0.7 SO_3^- groups/nm^2 of the pore wall. The quantitative estimates of σ are given in the Appendix.

Since the grafted groups in samples IV and V are not charged, it can be assumed that the surface charge density of the nanoparticles in these samples is approximately the same as in sample II with silica nanoparticles. The silica nanoparticles embedded in Sample III are functionalized by 3-aminopropyl moieties. The amino group attached to the particle surface (Fig. 2) is positively charged and accepts H^+ to form $-NH_3^+$. The surface charge density (estimated in the Annex) is between +0.11 and +0.24 (C m^{-2}), that is, it is equal to or higher than σ formed by the sulfonate groups attached to the pore walls.

As for the size of nanoparticles, it is influenced by two factors: the size of the pores where the particles are formed, and the substituents on the surface of silica introduced in functionalization. When mixing the Nafion solution with a precursor, the latter is distributed approximately uniformly, since condensation processes have not yet occurred. The treatment of the obtained film (after evaporation of the solvent) with a hydrolyzing agent causes the formation of nanoparticles in sufficiently large pores, with the formation of one particle per pore. Apparently, 2 or 3 particles cannot form in one pore as the pore size is small, and diffusion in the pore, which supplies the material for the formation of the particle, occurs extremely quickly. The thin channels limit the exchange between large pores (known also as clusters), they nearly isolate the reaction zones from each other. It is possible, however, that a part of the material for particle formation can

be delivered from the neighboring smaller pores. Thus, the impact of pore on the size of nanoparticle seems to be decisive [4].

On the other hand, the functionalization of the nanoparticles also has an effect. When a substituent joins a silicon atom, it prevents the formation of a strong covalent bond between the silicon and oxygen atoms and, therefore, blocks the growth of the nanoparticle core in size. We suppose that these limitations in the nanoparticle size occur in accordance with the mechanism of molecular weight regulation in polysiloxane synthesis where monofunctional groups are used as end-blockers for functionally terminated oligomers [52]. Therefore, addition of weak polar or nonpolar functional groups (as in the case of samples IV and V) may result in smaller size of nanoparticles. On the other hand, it is also known that amino-modified silica particles (in particular, aminopropyl-grafted silica as in sample III) form relatively large agglomerates due to interaction and bonding of amino groups with the silanol groups on the particle surface [53]. According to the above, we hypothesize that sample III contains the biggest immobilized nanoparticles; samples IV-V, the smallest ones; and sample II has the particles of the medium size. The latter is in the range 3-7 nm according to our TEM images (Fig. 3), which correlates with the results of Ref. [54] showing that this size can be as large as 8 nm. This is slightly greater than the size of the clusters (≈5 nm) in Nafion membranes [5,55], but is within the range of all possible pores, whose size can reach 100 nm, according to the method of standard contact porosimetry [55]. In the case of silica nanoparticles with 5 mol% of 3-aminopropyl groups on the surface, the diameter was estimated as 4 – 10 nm [56].

4.2. Membrane bulk-dependent characteristics

4.2.1. Model approaches to describing the IEM structure

The structure of Nafion-type ion-exchange membranes is usually described by the Gierke cluster-network model schematically presented in Fig. 4a. The membrane is considered as a system of hydrated clusters connected by narrow and short channels (diameter and length of about 1 nm) enclosed in a hydrophobic matrix. The fixed charges (SO_3^- groups) are located on the walls of the clusters, which have a shape close to spherical.

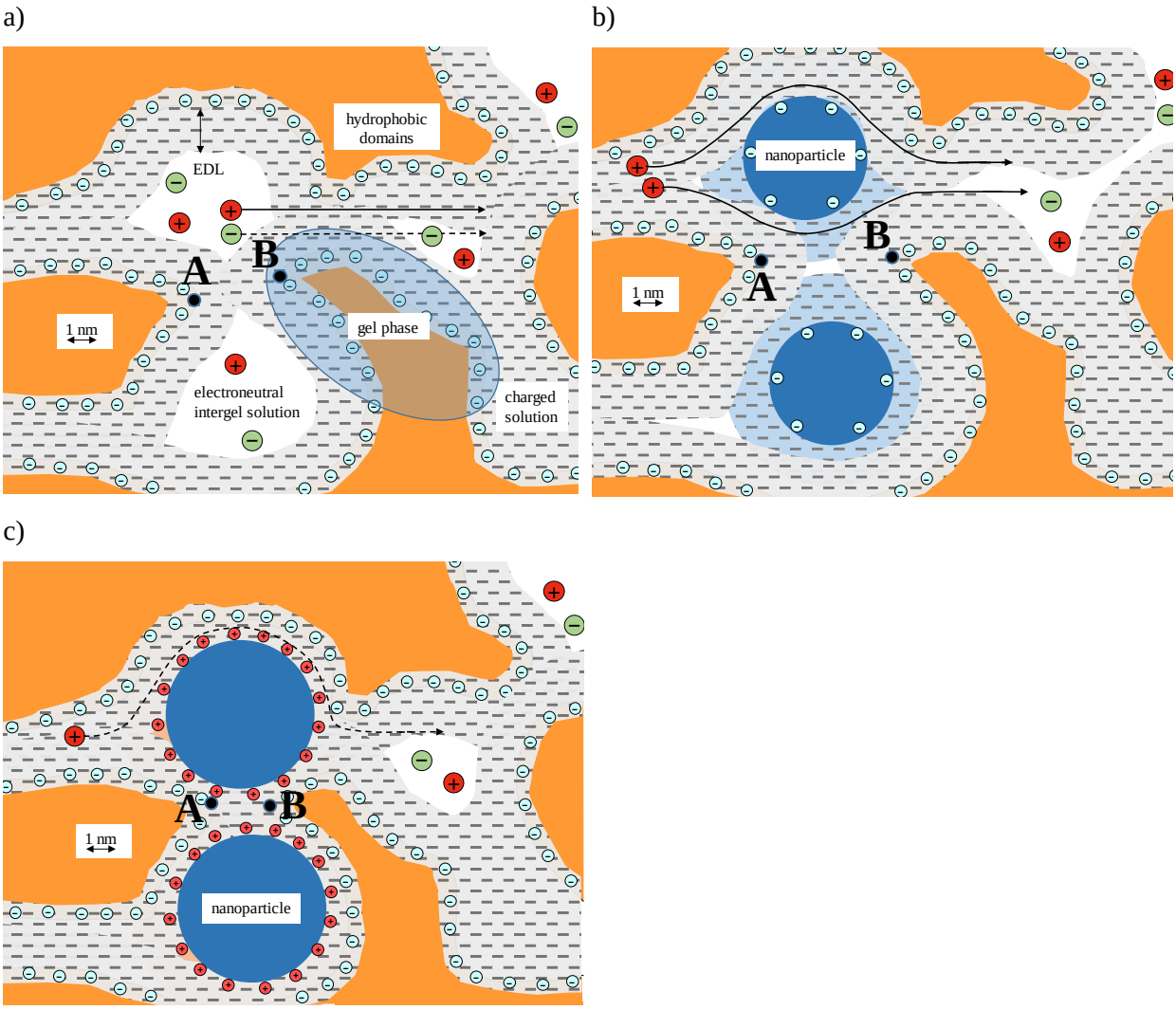

Fig. 4. Schemes representing the nanostructure of a Nafion-type membrane (a) and its modifications with incorporated nanoparticles in the case of negatively (b) and positively (c) charged surface. Negatively charged nanoparticles alter the pore structure so that relatively large non-selective pores are transformed into a network of thinner pores, in which the concentration of counterions is much higher than that of coions; at the same time, too thin pores/channels become larger pores (compare the distance between points A and B, which determine the size of an inter-cluster channel). Positively charged nanoparticles form salt bridges with fixed ions and block inter-cluster channels, making pores/channels narrower. In both cases, mesoporous structure of the pristine membrane is transformed into a microporous one.

Several approaches were developed to model the membrane transport properties as dependent on its nanostructure [57–62] (see description in the Supplementary materials).

The microheterogeneous model [57,58] gives a simple description of membrane transport characteristics (including the conductivity, diffusion permeability and transport numbers) as

functions of a single set of parameters, which are the diffusion coefficients in the gel and free solution phases, the volume fractions of the gel phase (f_1) and intergel spaces (f_2, $f_1 + f_2 = 1$), the Donnan equilibrium constant and a parameter (α), which reflects the relative disposition of the gel and solution phases [45].

4.2.2. Membrane conductivity

According to the microheterogeneous model [57], within the concentration range $0.1c_{iso}<c<10c_{iso}$, and under condition that parameter α is not too great ($|\alpha|\leq 0.2$), the electrical conductivity of an IEM, κ^*, and the concentration of the bathing solution, c, are related by the following equation:

$$\lg \kappa^* \approx f_2 \lg c + const \quad (1)$$

Here c_{iso} is the isoconductance concentration (the concentration at which the conductivity of the membrane and bathing solution is the same) [57]; usually for conventional IEMs, c_{iso} is close to 0.05-0.1 M.

The linearity of the $\lg(\kappa^*)$ - $\lg(c)$ dependence for conventional IEMs is confirmed in a number of publications [57,63]; parameter f_2 (the volume fraction of the intergel spaces) is easy to find as the slope of the above dependence. Most often the concentration dependence of the conductivity is measured in the 0.05 – 1 M range, where Eq. (1) is approximately satisfied. Besides, this range is most interesting for the practice, and the measurements there are relatively easy. However, sometimes this dependence is determined in a range outside of that where Eq. (1) holds; parameter α can be rather high (>0.2). In these conditions, the value of the $\lg(\kappa^*)$ - $\lg(c)$ slope can differ from the true volume fraction of the intergel spaces; this is especially the case where the intergel spaces contain nanoparticles. With that, the slope still roughly characterizes the presence of the electroneutral solution in the membrane, when the $\lg(\kappa^*)$ - $\lg(c)$ dependence is determined in the 0.05 – 1 M range [38]. We will call this slope the apparent fraction of the electroneutral solution in the membrane, f_{2app}. As Table 1 shows, the f_{2app} value (determined in the 0.03 – 0.5 M concentration range) significantly differs from one sample to other; its value can be used to characterize the presence of meso- and macropores in a membrane, as explained in section 4.1. Generally, f_{2app} shows how rapidly the conductivity increases with increasing concentration. At the same time, this parameter gives the real value of intergel spaces' volume fraction in the conditions described in the beginning of this section, namely, when the bathing solution concentration is sufficiently close to c_{iso} (as it was established in a number of papers [45,55,65]).

However, as Fig. 5 shows, in the range of very low concentrations (c<0.01 M), the $\lg(\kappa^*)$ - $\lg(c)$ dependence is no longer linear. This feature was also found in other publications [61,64].

This deviation from linearity follows from the microheterogeneous model [57]; however, in experiments, the 'flattening' of the $\lg(\kappa^*)$ - $\lg(c)$ curve is stronger than the original version of the model [57] predicts. As it was explained in [61,64], this flattening is due to the fact that the thickness of the EDL formed at pore walls increases with dilution of solution; a larger part of pore volume becomes more conductive than the equilibrium electroneutral solution.

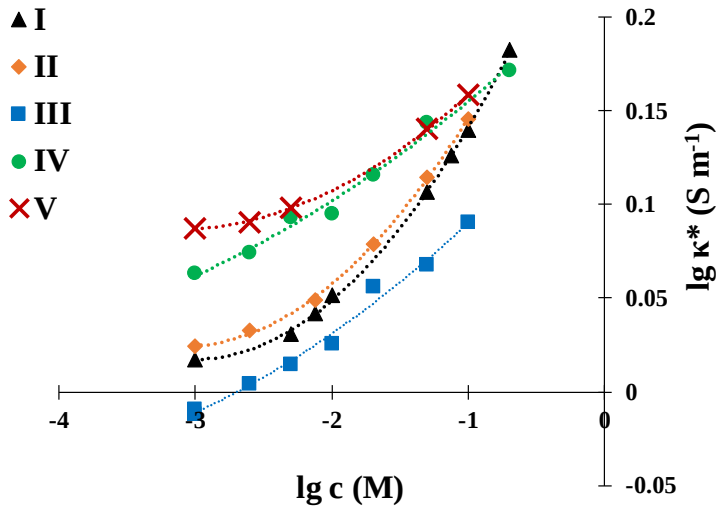

Fig. 5. Concentration dependences of electrical conductivity of the pristine Nafion membrane (sample I) and its modifications obtained by incorporation of silica-based nanoparticles (Table 1). The roman numerals show the numbers of samples. The values were determined with an uncertainty of 2%.

Interestingly, the nanoparticles affect the conductivity significantly stronger (Fig. 5) than it can be expected, given the low number of nanoparticles in the membranes (3 wt%). Moreover, the conductivity values for the same number of nanoparticles vary in a relatively large range depending on the type of functionalization. And the slope of the $\lg(\kappa^*)$ - $\lg(c)$ curves in the range 0.05 – 1 M, where the curves are approximately linear, depends on the functionalization. However, since the water uptake changes only little for the samples of different functionalization, we cannot expect that the pore size and shape vary significantly. That is, the volume fraction of the intergel spaces, f_2, must not change. However, the value of the apparent volume fraction of electroneutral solution, f_{2app} (the slope of the $\lg(\kappa^*)$ - $\lg(c)$ curve) is a sensitive parameter (Table 1). More likely that the nanoparticles occupy only relatively large pores, but they significantly affect the overall membrane porous structure. In the pores where they are present, they replace the electroneutral solution. The EDL around a nanoparticle enhances the membrane conductivity in the same way as

the EDL at the pore walls. The difference in the $\lg(\kappa^*)$ - $\lg(c)$ curves reflects the fact that the EDL around the nanoparticles depends on the functionalization.

Experimental data shows that in the range of low concentrations (0.001 - 0.2 M), the conductivity of most of the modified samples (except that for sample III) is greater than the conductivity of the non-modified Nafion membrane (sample I) (Fig. 5).

In the literature, two reasons for the conductivity increase caused by the incorporation of nanoparticles are discussed: (1) the higher size of membrane pores and conductive channels resulted by increasing osmotic pressure due to hydrophilic surface of nanoparticles (the limited membrane elasticity model [4,66]), (2) and the appearance of additional charge carriers due to formation of additional EDL at the charged surface of a nanoparticle [38,67]. According to the estimations above, the space charge density of all the nanoparticles used in this study (with the exception of those in sample III) should be close to each other at a given pH and external solution concentration. In these circumstances, the impact of the EDL formed around the particles on the membrane properties should be essentially determined by their size. The smaller the size of nanoparticles, the greater the total volume of EDL around them and, accordingly, the greater the amount of charge carriers and the osmotic pressure. This relationship might explain the relative position of the curves in Fig. 5: the conductivity, κ^*, of the samples in dilute solutions is in the same row ($\kappa^*_I \approx \kappa^*_{II} < \kappa^*_{IV} < \kappa^*_V$) as the size of nanoparticles estimated in Section 2. Sample III containing positively charged nanoparticles has the lowest conductivity, κ^*_{III}. Apparently, this is due to the electrostatic interactions between the positively charged amino groups and the negative fixed charges of the membrane. These salt bridges can cause (1) a decrease in current carriers' concentration in the mesopores; (2) convergence of the opposing pore walls and reduction in the pore size [11] (Fig. 4).

4.2.3. Diffusion permeability

A decrease in diffusion permeability, P^*, compared with the pristine Nafion membrane is observed for all modified specimens (Fig. 6). It is explained by the fact that the nanoparticles with their EDLs replace the electrically neutral solution (which is not a permselective medium) as well as reduce the space available for electrolyte diffusion in the pores. The lowest value of P^* is shown by sample III, evidently, because the positively charged nanoparticles in this membrane can block some conducting channels available for the transport of coions (Fig. 4c), which control the rate of electrolyte diffusion in IEMs [68]. In this case the counterions can pass through the gel phase bypassing the nanoparticles, while this way is nearly closed for the coions. Sample V also has a very low permeability towards NaCl diffusion, the main cause of which should be a relatively

large number of negatively charged nanoparticles of small size. This results in formation of a larger number of pathways hardly available for anions, as compared to other samples.

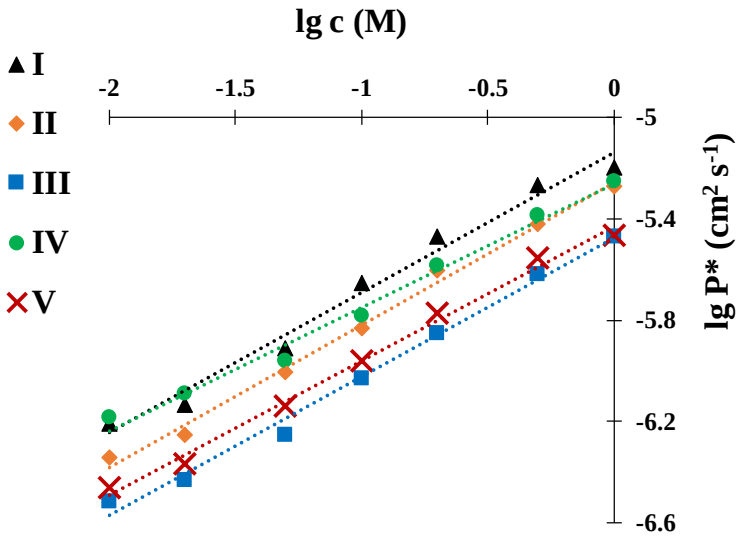

Fig. 6. Concentration dependences of diffusion permeability towards NaCl of a Nafion membrane and its modifications. The roman numerals show the numbers of samples. The values were determined with an uncertainty of 4%.

4.2.3. Transport numbers

An important parameter characterizing the membrane permselectivity is the counterion transport number, t_i^*. In the case of the studied cation-exchange membranes and sodium chloride solution, the value of t_+^* shows the portion of the electric current transferred by the Na^+ ion in conditions of the absence of diffusion. To evaluate the t_+^* value, it is possible to use the following relationship (deduced within the irreversible thermodynamics [69]), which relates the transport numbers, electrical conductivity and diffusion permeability:

$$t_-^* = \frac{F^2}{2RTg}\frac{P^* c}{\kappa^* t_{+app}^*} \qquad (2)$$

where $g = 1 + d\ln y_\pm / d\ln c$ is the activity factor, $y_\pm$ is the mean activity coefficient of the electrolyte; t_{+app}^* is the apparent transport number of counterions, which is linked with the true transport number in the membrane by the Scatchard equation [69]. As a first approximation, $t_{+app}^* \approx t_+^*$. In fact, t_{+app}^* is 10-15% lower than t_+^*, the difference increases with increasing water electroosmotic transport. Eq. (2) shows that t_-^* is proportional to the membrane diffusion permeability (controlled by the coion transport) and inversely proportional to the membrane conductivity (mainly determined by the counterions).

By applying the assumptions that $t^*_{+app} \approx t^*_+$ and parameter g is equal to 1, we obtain from Eq. (2) and condition $t^*_- + t^*_+ = 1$ a quadratic equation, the solution of which is as follows:

$$t^*_- = \frac{1}{2} - \sqrt{\frac{1}{4} - \frac{P^* F^2 C}{2RT\kappa^*}}, \qquad t^*_+ = 1 - t^*_- \tag{3}$$

To apply Eq. (3), the experimental concentration dependences of the electrical conductivity and diffusion permeability were approximated by a power function. Fig. 7 compares counterion transport numbers in the studied samples.

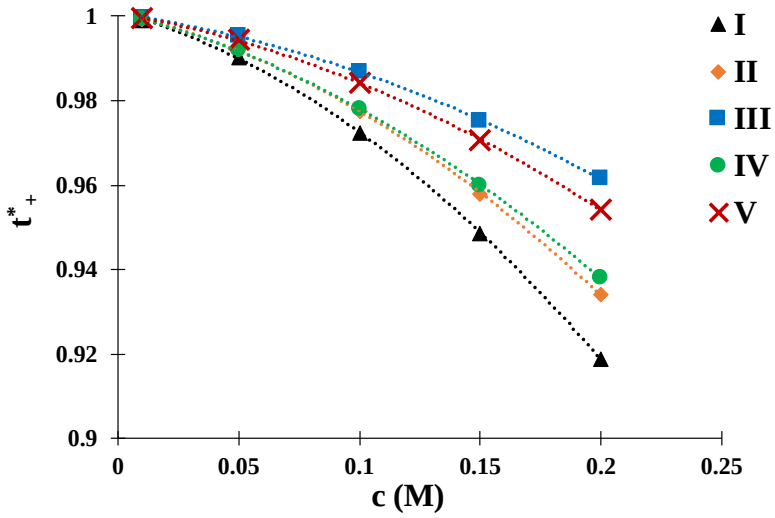

Fig. 7. Concentration dependences of the Na^+ transport numbers in the Nafion membrane (sample I) and its modifications. The roman numerals show the numbers of samples. The values were determined with an uncertainty of 1%.

As expected, the pristine membrane, sample I, has the lowest permselectivity (the smallest values of t^*_+) (Fig. 7). The t^*_+ values for this membrane are as well lower than the transport numbers in commercial Nafion® membranes. For example, interpolation of the results reported by in Ref. [69] for a Nafion®120 in 0.2 M NaCl gives $t^*_+ = 0.98 \pm 0.01$, while for sample I the corresponding value is close to 0.92 (Fig. 7). The reason of this difference is that in this study, sample I was prepared by a Nafion solution casting (Section 2, Materials). As mentioned in Section 2, the structure of sample I is essentially more porous, hence, more permeable to coions than that of commercial Nafion® membranes.

Interestingly enough, sample III has the highest selectivity despite its lowest conductivity. Apparently, the determining factor in this case is a very low value of diffusion permeability. This is caused by the positively charged nanoparticles, which act as a crosslinking agent and block the pathways for anions [11]. The effect of these nanoparticles on the restriction of ion transport is greater for coions than for counterions. In the case of 0.1 M NaCl solution, the value of P^* for

sample III is about 2.5 times lower than for sample I; however, the value of κ^* for sample III is only 1.1 times lower than that for sample I.

4.3. Membrane surface-dependent characteristics

4.3.1. Current-voltage characteristics and chronopotentiograms

While conductivity and diffusion permeability of a membrane are controlled by its bulk properties, current-voltage characteristics (CVC) and chronopotentiograms (ChP) are determined mainly by the membrane surface properties. The latter is due to the fact that generally the shapes of CVC and ChP are determined by the development of concentration polarization in the membrane system with growing potential difference/current density. Concentration polarization causes two current-induced coupled effects: electroconvection and water splitting, both depending only on surface properties. It was shown in the literature, that the shape of CVC of an IEM depends on the relative hydrophilicity/hydrophobicity of its surface (characterized by the contact angle) [70], surface electric and geometric heterogeneity [70–74] and the surface charge density [75]. Since the surface geometry/morphology (determining electric and geometrical heterogeneity) does not change from one sample to another, this factor can be ignored in our analysis. As for the contact angle, within the experimental error, it is the same for all samples except for sample III. The lower value of the contact angle for this sample should be due to the fact that the surface of the nanoparticles is positively charged, which decreases the overall membrane charge density.

As Fig. 8 shows, the CVC of studied membranes in the range $0.6 < i/i_{lim} < 1$ (0.03 V<$\Delta\varphi'$<0.2 V) are positioned in the same row as their conductivities. Here $\Delta\varphi'$ is the corrected potential drop not including the ohmic contribution [76]. Both the current densities at a fixed $\Delta\varphi'$ and the conductivities increase in the same order: III<I≈II<IV<V (Table 2).

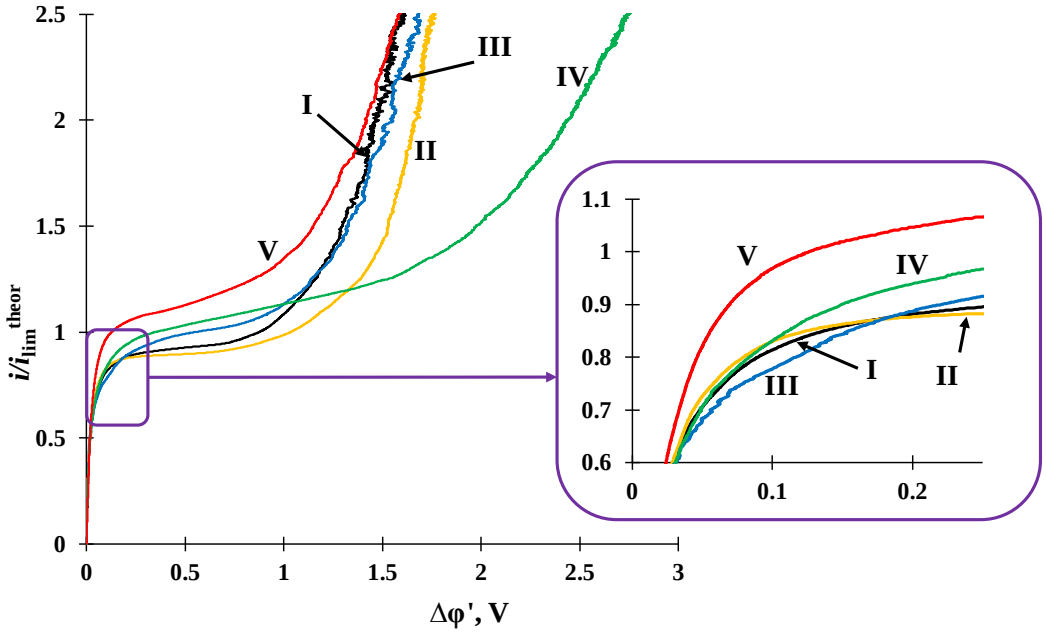

Fig. 8. Current-voltage characteristics of the studied membranes in a 0.02 M NaCl solution. The roman numerals show the sample numbers. The values were determined with an uncertainty of 5%.

Table 2. Some electrochemical characteristics of studied membranes. The Arabic numbers in brackets place the samples from best (1) to worst (5).

Samples	Conductivity (S m^{-1}), κ^*, (c=0.001 M NaCl)	i/i_{lim} ($\Delta\varphi'$=0.1V)	τ/τ_{Sand} (i/i_{lim}=1.5)
I	1.04 (4)	0.95 (4)	1.04 (5)
II	1.06 (3)	0.97 (2-3)	1.07 (3)
III	0.98 (5)	0.91 (5)	1.06 (4)
IV	1.16 (2)	0.97 (2-3)	1.08 (2)
V	1.22 (1)	1.13 (1)	1.14 (1)

The uncertainty for the values of κ^*, i/i_{lim} and τ/τ_{Sand} is evaluated as 0.015 S m^{-1}, 0.01 and 0.01, respectively.

The shape of the CVC in the indicated range of currents/potentials is strongly influenced by equilibrium electroconvection [77], which occurs as electroosmosis (EO) of the first kind [78]. The latter phenomenon is conditioned by the space charge region (SCR) in the depleted solution adjacent to the membrane surface. The term “equilibrium EO” is used [77] because at underlimiting current densities and low potential drops, the structure of the SCR is similar to that of the equilibrium EDL occurring at zero current. Namely, the counterion and coion concentrations are distributed there according to the Boltzmann law. Electroconvection enhances the mass

exchange at the surface: it brings a “fresh” solution from the bulk and evacuates the depleted solution. Thus, a more intensive electroconvection enables a higher current density under the same potential difference. Apparently, the surface charge of embedded nanoparticles contributes to the formation of a space charge region in the solution not only within the pore, but also at the external membrane surface. The total amount of the charged solution, which is due to the presence of nanoparticles, depends on the surface charge density and the number of the nanoparticles per membrane unit volume. Since the total mass of nanoparticles is the same in all samples (3 wt.%), the greater the nanoparticle’s surface charge density and the smaller the particle size, the greater the charged solution amount per unit volume and per unit area of the internal or external pore wall surface. Therefore, both membrane conductivity and equilibrium electroconvection enhancing the current density increase in the same order of the studied samples: III<I≈II<IV<V (Table 2).

In the case of sample III, the nanoparticles contain amino groups, which are charged positively, that is oppositely to the membrane fixed sulfo groups. As a result of the electrostatic interaction between the amino groups and the fixed sulfo groups, a part of sulfo groups would be blocked and the average fixed charge density of the membrane pore walls and that of the membrane surface should be lower than in the pristine Nafion and other modified samples. This causes both a lower conductivity and a lower current density for sample III. In addition, this sample is the most hydrophilic among the studied samples. This property hampers the EO slip along the membrane surface. Inversely, in the case of nanoparticles with a negatively charged surface, the surface charge of the modified membranes should be higher than that of the pristine membrane; and the less the size of nanoparticles, the greater the surface charge.

Intrestingly, the above correlation occurs only at low current densities (from $0.6\, i/i_{lim}$ to $1.0\, i/i_{lim}$) and low potential differences. At higher currents/voltages, the order of the samples for which the current density increases at a fixed potential drop is different. While sample V remains the best at high currents, sample IV, the second in the competition of conductivity and limiting current densities, requires the highest voltage to allow the passage of a current density $i \geq 2\ i_{\text{lim}}$. Evidently, the laws governing electroconvection phenomenon at low currents/voltages are not the same as those at intensive currents and high voltages. The mechanism of electroconvection at relatively high current densities is apparently determined to a lesser extent by EO slip than at current densities close to i_{lim} [78–80]. As it is explained in Section 4.3.2, water splitting acts an important roleб since it partially suppresses electroconvection.

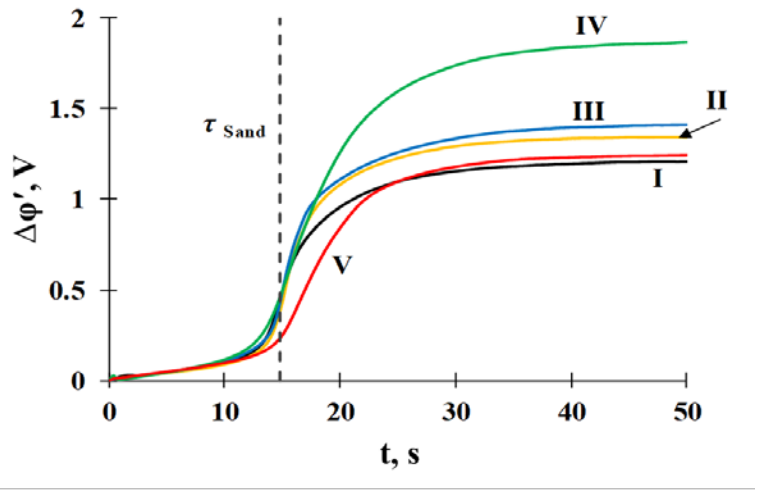

Fig. 9. Chronopotentiograms of the studied membranes measured at i=1.5 i_{lim}=1.97 in a 0.02 M NaCl solution. The roman numerals show the sample numbers. The values were determined with an uncertainty of 5%.

The analysis of chronopotentiograms provides additional evidence of the correlation between membrane conductivity and electroconvection at low currents/potential drops. The inflection point of a chronopotentiogram (Fig. 9) refers to the transition time, τ [81], which is an important parameter determining the time required to the electrolyte concentration at the membrane surface to achieve a nearly zero value. The τ/τ_{sand} values are presented in Table 2, where τ_{sand} is the theoretical value of transition time calculated using the Sand equation [82]:

$$\tau_{Sand} = \frac{\pi D}{4}\left(\frac{Fz_1C_1}{T_1-t_1}\right)^2 \frac{1}{i^2} \quad (4)$$

where C_1 is the counterion concentration in the bulk solution; T_1 and t_1 are the counterion transport numbers in the membrane and solution, respectively; z_1 is the counterion charge number; F is the Faraday constant; and i is the current density.

The Sand theory [82] assumes that a stagnant diffusion layer of infinite thickness is adjacent to an ion-permselective surface. However, a significant current-induced convection arises at the charged surface of ion-exchange membranes, when the near-surface concentration of electrolyte reaches a sufficiently small value. In particular, electroosmosis of the first kind (equilibrium electroconvection) develops without threshold and becomes noticeable even at small potential drops, $\Delta\varphi'$, about 50 mV when subtracting the ohmic contribution [75]. The electroosmotic flow enhances mass exchange at the surface, which results in increasing τ. Thus, the same phenomenon, equilibrium electroconvection, is behind the increase in the steady-state current density when measuring the CVC and in the increase in transition time. Both the current

and the transition time increase occur in the same range of relatively low potential differences between 50 and 200 mV. Therefore, it is not surprising that the sequence of τ/τ_{sand} values is in the same order as the current density, which in turn, correlates with the membrane conductivity (Table 2).

4.3.2. Interplay between electroconvection and water splitting

There is another interesting issue, which can be discussed on the basis of the results presented above and shown in Fig. 10. This figure displays the pH difference, ΔpH, between the output and input solution, which passes through the desalination compartment, as a function of the corrected potential drop $\Delta\varphi'$. Water splitting (WS) occurs in the surface layer of both anion-exchange (AEM) and cation-exchange (CEM) membranes [83], and both processes contribute to the pH change: WS in the AEM delivers protons into the desalination compartment, that in the CEM, hydroxyls (Fig. 11). The value of the output solution pH depends on the difference in the WS rates in the AEM and CEM. Since in all experiments, the same MA-41 anion-exchange membrane was used, it is possible to compare the WS rate in different samples of CEMs. The higher the ΔpH value, the higher the WS rate in the considered sample of CEM.

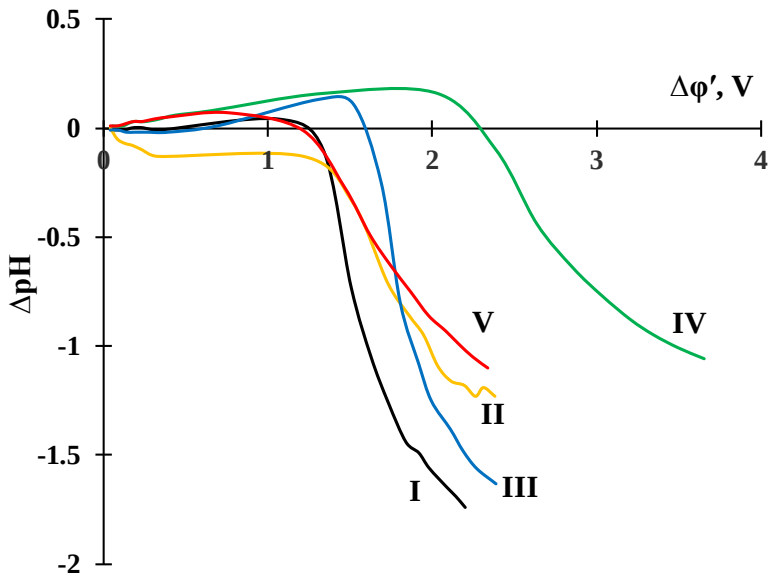

Fig. 10. Dependence of the pH difference between the outlet and inlet solution passing through the desalination chamber on the corrected potential difference in a 0.02 M NaCl solution. The roman numerals show the sample numbers. The values were determined with an uncertainty of 0.02.

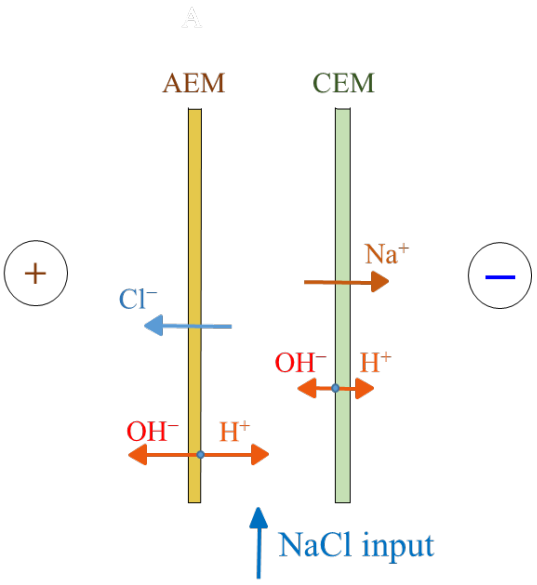

Fig. 11. Scheme of fluxes of salt and water ions in the desalination compartment of an ED cell; the case where WS rate at the AEM is greater than that at the CEM.

The interplay between electroconvection and WS was discussed in a number of papers [73,80,84–89]. The onset of both electroconvection and WS requires the occurrence of a depleted solution region at the membrane surface where a space charge region is formed. For electroconvection, the presence of a SCR, which can be moved under the action of an external electric field, is necessary. As for WS, since the co-ions are expelled from the SCR, this leads to displacement of the equilibrium between the dissociation and recombination reactions resulting in WS. Low values of the product of H^+ and OH^- concentrations are necessary to hold inequality $c_H c_{OH} < (K_w)^2$, where $K_w = 10^{-14}$ $(mol/L)^2$ is the water dissociation constant. The region where inequality $c_H c_{OH} < (K_w)^2$ holds is known as the reaction region. As mathematical modelling shows, the reaction region practically coincides with the SCR both in the case of bipolar [90] and monopolar membranes. In the case of bipolar membranes, the SCR 1-2 nm thick is located in the vicinity of the bipolar junction; in the case of monopolar membranes, the SCR includes a nanosized equilibrium EDL at the membrane interface and an extended SCR in the depleted solution, which can reach several micrometers. Near a CEM, the SCR almost does not contain anions; therefore, the concentration of the OH^- ions there is very small and the inequality $c_H c_{OH} << (K_w)^2$ is valid throughout the SCR. To attain a sufficiently thick SCR, the electrolyte concentration near the membrane, c_s, should be quite low. The thickness of the (quasi-)equilibrium EDL is inversely proportional to $(c_s)^{0.5}$; the value of c_s should be of the order of 10^{-5} mol/L or lower in order that the H^+ (OH^-) ions could compete with the salt ions in the charge transfer. Note also that a relatively strong electric field within the SCR is favorable not only for EC, but for WS as well, due to the second Wien effect enhancing the water splitting rate [83,85,91,92].

However, when the conditions for the onset of electroconvection and WS are reached, these two phenomena become antagonist. Intensive electroconvection brings fresh electrolyte solution from the solution bulk, which prevents the development of WS. Intensive WS produces the H^+ (OH^-) ions, which enter the SCR as coions and reduce the space charge in depleted solution at the membrane surface [80,85]. The presence of a catalyst for water dissociation can essentially shift favorable conditions towards WS [83,91] and suppress electroconvection [85,87,93].

As can be seen in Fig. 10, all ΔpH vs. $\Delta\varphi'$ curves have a similar shape. Between 0.5V and 1.5V, there is a slight maximum in ΔpH value. Then ΔpH decreases. An increase in pH of the feed solution after passing the desalination compartment is due to the fact that at relatively low potential drops the rate of WS is higher in the CEM than in the AEM because the limiting current density for the CEM is about 1.5 times lower than that for the AEM. Hence, with increasing i (and $\Delta\varphi'$), the limiting current density is first attained at the CEM, where WS starts to occur with a noticeable rate, while there is no WS in the AEM. However, with a further increase in i ($\Delta\varphi'$), the limiting current density is reached at the AEM, and WS starts in this membrane. The CEMs under study (a Nafion membrane and its modifications), mainly contains functional sulfo groups, whose catalytic activity in respect to WS is very weak [94]. For this reason, the increase in pH of the desalting solution (in the 0.5V - 1.5V range) is quite low even if WS does not occur in the AEM. At the same time, among the functional groups of the AEM (MA-41 membrane), there are secondary and tertiary amino groups, which are catalytically active for WS. Thus, when the current density becomes equal to or greater than the limiting current density for this membrane, the rate of WS in the AEM, which supplies the H^+ ions into the desalination compartment, exceeds the WS rate in the CEM. Then the pH of the output solution decreases rapidly with increasing $\Delta\varphi'$ (Fig. 10).

It can be seen that for all modified membranes, the water splitting is higher than for the pristine membrane: the ΔpH *vs.* $\Delta\varphi'$ curves for all modified membranes are over the curve for sample I (Fig. 10). Apparently, it is due to catalytic participation of the functional groups of nanoparticles in the proton-transfer reactions leading to water splitting [83]. The weak-acid −SiOH groups of silica particles with $pK_a \approx 6.4$ should be a good catalyst for the water dissociation reaction, in contrast to the $-SO_3H$ groups, for which $pK_a \approx 1.5$ (for weakly-acid functional groups, the limiting rate constant of WS in the first approximation is inversely proportional to K_a [83]). The functionalization affects the catalytic activity of nanoparticles towards WS. The WS rate at the CEM in the range $\Delta\varphi' > 1.2$ V for the studied samples increases in the order: I < III ≈ II ≈ V < IV. With this, among the modified samples, there is a significant difference between samples V and IV. Perhaps, this is due to the fact that sample IV contains nonpolar propyl groups, and sample V, weak polar 3,3,3-trifluoropropyl groups. Generally, the order of samples regarding the CVC and

ΔpH *vs.* Δφ′ dependencies can be explained by the discussed above antagonism between electroconvection and WS phenomena. Indeed, as follows from Fig. 10, sample I is characterized by the lowest catalytic activity of functional groups in respect to WS; the catalytic activity of functional groups of sample IV is the highest. Accordingly, it can be expected that the intensive WS at high potential drops suppresses partially electroconvection. It seems that at elevated Δφ′ (>1.2 V), the other membrane characteristics, such as surface space charge density and hydrophobicity act a secondary role. If we take sample III, the worst in terms of conductivity, it should have the lowest surface space charge density. At Δφ′=0.1 V, the current density is the lowest for this sample. However, at Δφ′ >1.5 V, the value of *i* is nearly the same as for samples V and I, showing the highest values of *i*; this should be due to relatively low WS rate for this membrane.

Conclusion

The introduction of nanoparticles with negatively charged surface leads to increasing the membrane conductivity and permselectivity while reducing the electrolyte diffusion permeability. This effect can be explained by transformation of the mesoporous membrane structure into a microporous one, accompanied by an increase in the inter-cluster channels' size. A negatively charged nanoparticle should be located in the center of a cation-exchange membrane pore due to electrostatic repulsion between its surface and the fixed sulfonate groups on the pore walls. Thus, the electroneutral solution in the center of a mesopore in the pristine membrane is displaced by the nanoparticle and its EDL. The counterions in the EDL contribute to increasing the conductivity, while the Donnan exclusion of co-ions inhibits the electrolyte diffusion. Increasing osmotic pressure in the membrane porous solution leads to enlarge the porous space.

The functionalization of silica particles with 3-aminopropyl imparts them a positive charge. There are electrostatic interactions between this charge and the fixed sulfonate groups; salt bridges can be formed. As a result, a part of fixed groups becomes blocked; with that, the nanoparticles can plug the narrow channels connecting greater pores. This design leads to a slight decrease (by about 10% compared to the pristine membrane) in the membrane conductivity and a significant (about 2.5 times) decrease in electrolyte diffusion, resulting in a considerable increase in the counterion permselectivity.

There is a correlation between the conductivity, κ^*, transition time, τ, and current density, *i* (measured at a fixed reduced potential difference, $\Delta\varphi'$, in the range 0.03 V<$\Delta\varphi'$<0.2 V) for the samples obtained from a Nafion-type membrane by its modification with silica nanoparticles. The samples differ by different functionalization of the nanoparticles. All three characteristics increase

from sample to sample in the same order: III<I≈II<IV<V. This correlation can be explained by the fact that the total space charge (TSC) around all nanoparticles embedded in a unit membrane volume increases from sample to sample in the order indicated above. The TSC value depends both on the space charge density of a nanoparticle and on their number per unit volume (surface). The greater the TSC, the larger the values of κ^*, τ and i , since the TSC

1) within the membrane pores contributes to increasing the concentration of mobile ions, hence, enhances the membrane conductivity, and
2) on the external membrane surface contributes to enhancing equilibrium electroconvection (electroosmosis of the first kind), which is significant in the range of potential drops from 0.03 V to 0.2 V. A more intensive electroconvection causes an increase in i and τ.

However, at $\Delta\varphi'$>1.2V, the order of samples for which i (measured at a fixed $\Delta\varphi'$) increases, is different. It is explained by the change in the mechanism of electroconvection from equilibrium electroosmosis to the non-equilibrium unstable electroconvection at high voltages. It seems that to achieve a high mass transfer rate at $\Delta\varphi'$>1.2V, the value of the surface charge density is no longer the main parameter. Perhaps, more important becomes the rate of water splitting. Generation of H^+ and OH^- ions in the solution/membrane interface leads to a reduction of the extended space charge in the depleted solution, which results in a partial suppression of electroconvection. The WS rate for all modified samples is higher than that for the non-modified Nafion membrane. Apparently, it is due to weakly acidic silanol −SiOH groups. Generally, electroconvection and WS are antagonists: strong WS essentially reduces electroconvection; and, conversely, intensive electroconvection delivers the fresh solution from the bulk to the depleted surface and thus prevents the development of WS.

Acknowledgments: This study was realized within a RFBR project (Ref. #20-58-12018 NNIO_a).

Appendix

Evaluation of the surface charge density of the nanoparticles

All modified samples studied in this paper contained silica nanoparticles with silanol acidic groups (-Si-O-H) on their surface. The pK_a value of these groups depends on the moieties bonded to Si. In the case of orthosilicic acid $Si(OH)_4$ in water, pK_a=9.8 [39]. However, in the case of a silica oxide nanoparticle in aqueous solution, pK_a is essentially lower: pK_a=6.4 according to

[32,33] and pK_a=6.8 according to [35], since $Si(OH)_4$ in these materials is subject to olation and oxolation processes. In acidic solutions, SiOH group can be protonated and positively charged. The equilibrium of the surface protonation-deprotonation reactions $SiOH \leftrightarrow SiO^- + H^+$ and $SiOH + H^+ \leftrightarrow SiOH_2^+$ [95] is characterized by the equilibrium constants K_a and K_b, respectively. Setting pK_a =6.4 [33] for the above equilibriums, we find that at pH=6 (the conditions of our experiment), $c_{SiOH^-} / c_{SiOH} \approx 0.4$ and $c_{SiOH_2^+} / c_{SiOH} \approx 10^{-8}$. Therefore, a significant part of the SiO_2 nanoparticles bears negative charges, the amount of the positively charged sites on the nanoparticle surface for the conditions of our experiments is negligible. Taking into account that the total number of sites on the surface $N_{s\,tot} = N_{SiO^-} + N_{SiOH}$ (where N_{SiO^-} and N_{SiOH} are the numbers of the SiO^- and SiOH sites, respectively), we find that the fraction of the negatively charged sites, f_-, is less than 30%. A more accurate evaluation on the basis of the Poisson-Boltzmann equations applied in the nanoparticle's EDL [33] and when using more sophisticated models taking into account the solvent electrostatics [34,35] gives f_- in the range 5 – 10% when the electrolyte concentration in the bulk is between 10^{-3} M and 10^{-1} M. In these models, it is accounted that the H^+ concentration at the surface is higher than in the solution bulk due to the electrostatic attraction between these ions and the negatively charged surface. Otherwise, the value of f_- can be also evaluated from the results of Sonnefeld et al. [32], who found from electrokinetic experiments that the SCD of a silica nanoparticle, σ, is between −0.01 and −0.025 C m^{-2} when the NaCl concentration is in the range from 10^{-3} M to 10^{-1} M and pH=6; the absolute value of σ increases with increasing the electrolyte concentration. According to Zhuravlev [96,97], the total site density of the silanol functional groups on the nanoparticle surface, α_{tot}, as determined by the deuterio-exchange method with mass spectrometric analysis is 4.6 sites nm^{-2} (i.e. $N_{s\,tot}$ =7.7×10^{-6} mol m^{-2}). At 0.01 M NaCl and pH=6, σ≈ −0.02 C m^{-2} [32], which amounts to α_-=0.125 charged sites per nm^2. Then f_- = 0.125/4.6 ≈ 0.03, hence, about 3% of sites on a SiO_2 nanoparticle are charged negatively. Note that the average distance between the fixed ions in Nafion membranes is about 1.2 nm (which gives the exchange capacity equal to 1 mol L^{-1} of swollen membrane). Then the density of the fixed charges on a pore wall, α_{SO3-}, will be 0.7 SO_3^- groups/nm^2, and the surface charge density $\sigma=(\alpha_{SO3-})e$ = 0.11 C m^{-2}, where e=1.60×10^{-19} C is the elementary charge. Thus, the charge density of the nanoparticle is about 5 times lower than that of the pore wall.

The silica nanoparticles embedded in Sample III are functionalized by 3-aminopropyl moieties. The amino group attached to the particle surface (Fig. 2) is positively charged and accepts H^+ to form $-NH_3^+$. The pK_a value for the reaction $NH_4^+ = NH_3 + H^+$ in aqueous solution is 9.25 [98], the pK_a value for aminopropyl $\equiv Si–(CH_2)_3–NH_2$ is 9.8 [99]. Therefore, at pH=6, almost all weakly basic amino groups are protonated and carry a positive charge. The number of these

positive charges is 5% of the total number of sites in one particle, $N_{v\,tot}$ (5%, i.e. $N_{v+} = 0.05\ N_{v\,tot}$). The positive charge surface density depends on the radius of the particle, r. $N_{v\,tot}$ is linked with the particle volume, V_p, as $N_{v\,tot} = V_p/V_{site}$, where the volume of a site may be approximately evaluated as L^3 with $L=(1/\alpha_{tot})^{1/2}$ (≈0.47 nm), the distance between two neighboring Si atoms. Then the site density of the positively charged groups on the nanoparticle surface, α_+, can be expressed as $\alpha_+ = \frac{N_{v+}}{S_p} = \frac{0.05V_p}{S_p L^3} = \frac{0.05r}{3L^3}$. When taking r=5 nm and 10 nm, we find α_+ equal to 0.82 and 1.64 (sites/nm^2), respectively; the surface charge density for these cases, $\sigma=(\alpha_+ - \alpha_-)e$, would be 0.11 and 0.24 (C m^{-2}), respectively. Therefore, it can be expected that the surface charge density of the nanoparticles in sample III is positive, the surface charge density is close to that on the pore walls and essentially higher in absolute value than the negative charge of a non-functionalized silica nanoparticle. The positive charges on the nanoparticles in sample III can play important role, taking also into account that the chain –$(CH_2)_3$-N is relatively long (about 0.7 nm). Note, however, that the above estimations are rather the upper limit, since they do not take into account that, due to the positive charge of the nanoparticle surface, the concentration of H^+ ions at the nanoparticle surface is significantly lower than in the bulk solution.

References

[1] J. Ran, L. Wu, Y. He, Z. Yang, Y. Wang, C. Jiang, L. Ge, E. Bakangura, T. Xu, Ion exchange membranes: New developments and applications, J. Membr. Sci. 522 (2017) 267–291. doi:10.1016/j.memsci.2016.09.033.

[2] T. Xu, Ion exchange membranes: State of their development and perspective, J. Membr. Sci. 263 (2005) 1–29. doi:10.1016/j.memsci.2005.05.002.

[3] Y. Gu, R.M. Dorin, U. Wiesner, Asymmetric organic-inorganic hybrid membrane formation via block copolymer-nanoparticle co-assembly, Nano Lett. 13 (2013) 5323–5328. doi:10.1021/nl402829p.

[4] P.Y. Apel, O. V. Bobreshova, A. V. Volkov, V. V. Volkov, V. V. Nikonenko, I.A. Stenina, A.N. Filippov, Y.P. Yampolskii, A.B. Yaroslavtsev, Prospects of Membrane Science Development, Membr. Membr. Technol. 1 (2019) 45–63. doi:10.1134/S2517751619020021.

[5] K.A. Mauritz, J.T. Payne, [Perfluorosulfonate ionomer]/silicate hybrid membranes via base-catalyzed in situ sol-gel processes for tetraethylorthosilicate, J. Membr. Sci. 168 (2000) 39–51. doi:10.1016/S0376-7388(99)00305-1.

[6] N. Miyake, J.S. Wainright, R.F. Savinell, Evaluation of a Sol-Gel Derived Nafion/Silica

Hybrid Membrane for Polymer Electrolyte Membrane Fuel Cell Applications: II. Methanol Uptake and Methanol Permeability, J. Electrochem. Soc. 148 (2001) A905. doi:10.1149/1.1383072.

[7] C. Laberty-Robert, K. Vallé, F. Pereira, C. Sanchez, Design and properties of functional hybrid organic-inorganic membranes for fuel cells, Chem. Soc. Rev. 40 (2011) 961–1005. doi:10.1039/c0cs00144a.

[8] M. Mika, M. Paidar, B. Klapste, M. Masinova, K. Bouzek, J. Vondrak, Hybrid inorganic-organic proton conducting membranes for fuel cells and gas sensors, J. Phys. Chem. Solids. 68 (2007) 775–779. doi:10.1016/j.jpcs.2007.02.052.

[9] I.A. Stenina, A.B. Yaroslavtsev, Nanomaterials for lithium-ion batteries and hydrogen energy, Pure Appl. Chem., 89 (2017) 1185–1194. doi:10.1515/pac-2016-1204.

[10] N.H. Jalani, K. Dunn, R. Datta, Synthesis and characterization of Nafion®-MO2 (M = Zr, Si, Ti) nanocomposite membranes for higher temperature PEM fuel cells, Electrochim. Acta. 51 (2005) 553–560. doi:10.1016/j.electacta.2005.05.016.

[11] D. V. Golubenko, R.R. Shaydullin, A.B. Yaroslavtsev, Improving the conductivity and permselectivity of ion-exchange membranes by introduction of inorganic oxide nanoparticles: impact of acid–base properties, Colloid Polym. Sci. 297 (2019) 741–748. doi:10.1007/s00396-019-04499-1.

[12] F. Pereira, K. Vallé, P. Belleville, A. Morin, S. Lambert, C. Sanchez, Advanced Mesostructured Hybrid Silica−Nafion Membranes for High-Performance PEM Fuel Cell, Chem. Mater. 20 (2008) 1710–1718. doi:10.1021/cm070929j.

[13] K.T. Adjemian, S.J. Lee, S. Srinivasan, J. Benziger, A.B. Bocarsly, Silicon Oxide Nafion Composite Membranes for Proton-Exchange Membrane Fuel Cell Operation at 80-140°C, J. Electrochem. Soc. 149 (2002) A256. doi:10.1149/1.1445431.

[14] F. Niepceron, B. Lafitte, H. Galiano, J. Bigarré, E. Nicol, J.F. Tassin, Composite fuel cell membranes based on an inert polymer matrix and proton-conducting hybrid silica particles, J. Membr. Sci. 338 (2009) 100–110. doi:10.1016/j.memsci.2009.04.022.

[15] A. Alabi, A. AlHajaj, L. Cseri, G. Szekely, P. Budd, L. Zou, Review of nanomaterials-assisted ion exchange membranes for electromembrane desalination, Npj Clean Water. 1 (2018). doi:10.1038/s41545-018-0009-7.

[16] S.M. Hosseini, N. Rafiei, A. Salabat, A. Ahmadi, Fabrication of new type of barium ferrite/copper oxide composite nanoparticles blended polyvinylchloride based heterogeneous ion exchange membrane, Arab. J. Chem. (2018). doi:10.1016/j.arabjc.2018.06.001.

[17] L.Y. Ng, A.W. Mohammad, C.P. Leo, N. Hilal, Polymeric membranes incorporated with

metal/metal oxide nanoparticles: A comprehensive review, Desalination. 308 (2013) 15–33. doi:10.1016/j.desal.2010.11.033.

[18] M. Nemati, S.M. Hosseini, E. Bagheripour, S.S. Madaeni, Electrodialysis heterogeneous anion exchange membranes filled with TiO2 nanoparticles: Membranes' fabrication and characterization, J. Membr. Sci. Res. 1 (2015) 135–140. doi:10.22079/jmsr.2015.14485.

[19] Y. Berbar, Z.E. Hammache, S. Bensaadi, R. Soukeur, M. Amara, B. Van der Bruggen, Effect of functionalized silica nanoparticles on sulfonated polyethersulfone ion exchange membrane for removal of lead and cadmium ions from aqueous solutions, J. Water Process Eng. 32 (2019) 100953. doi:10.1016/j.jwpe.2019.100953.

[20] N. Hilal, A.F. Ismail, C. Wright, Membrane Fabrication, CRC Press, 2015. doi:10.1201/b18149.

[21] X. Li, J. Li, B. Van der Bruggen, X. Sun, J. Shen, W. Han, L. Wang, Fouling behavior of polyethersulfone ultrafiltration membranes functionalized with sol–gel formed ZnO nanoparticles, RSC Adv. 5 (2015) 50711–50719. doi:10.1039/C5RA05783C.

[22] A. Tiraferri, Y. Kang, E.P. Giannelis, M. Elimelech, Highly Hydrophilic Thin-Film Composite Forward Osmosis Membranes Functionalized with Surface-Tailored Nanoparticles, ACS Appl. Mater. Interfaces. 4 (2012) 5044–5053. doi:10.1021/am301532g.

[23] H. Zhang, H. Zhang, X. Li, Z. Mai, W. Wei, Silica modified nanofiltration membranes with improved selectivity for redox flow battery application, Energy Environ. Sci. 5 (2012) 6299–6303. doi:10.1039/C1EE02571F.

[24] M. Paidar, V. Fateev, K. Bouzek, Membrane electrolysis—History, current status and perspective, Electrochim. Acta. 209 (2016) 737–756. doi:10.1016/j.electacta.2016.05.209.

[25] T. Sun, Y.S. Zhang, B. Pang, D.C. Hyun, M. Yang, Y. Xia, Engineered nanoparticles for drug delivery in cancer therapy, Angew. Chemie - Int. Ed. 53 (2014) 12320–12364. doi:10.1002/anie.201403036.

[26] Y. Wang, Q. Zhao, N. Han, L. Bai, J. Li, J. Liu, E. Che, L. Hu, Q. Zhang, T. Jiang, S. Wang, Mesoporous silica nanoparticles in drug delivery and biomedical applications, Nanomedicine Nanotechnology, Biol. Med. 11 (2015) 313–327. doi:10.1016/j.nano.2014.09.014.

[27] Y. Fan, P. Wang, Y. Lu, R. Wang, L. Zhou, X. Zheng, X. Li, J.A. Piper, F. Zhang, Lifetime-engineered NIR-II nanoparticles unlock multiplexed in vivo imaging, Nat. Nanotechnol. 13 (2018) 941–946. doi:10.1038/s41565-018-0221-0.

[28] L.L. Israel, A. Galstyan, E. Holler, J.Y. Ljubimova, Magnetic iron oxide nanoparticles for imaging, targeting and treatment of primary and metastatic tumors of the brain, J. Control.

Release. 320 (2020) 45–62. doi:10.1016/j.jconrel.2020.01.009.

[29] K.F.L. Hagesteijn, S. Jiang, B.P. Ladewig, A review of the synthesis and characterization of anion exchange membranes, J. Mater. Sci. 53 (2018) 11131–11150. doi:10.1007/s10853-018-2409-y.

[30] J. Miao, L. Yao, Z. Yang, J. Pan, J. Qian, T. Xu, Sulfonated poly(2,6-dimethyl-1,4-phenyleneoxide)/nano silica hybrid membranes for alkali recovery via diffusion dialysis, Sep. Purif. Technol. 141 (2015) 307–313. doi:10.1016/j.seppur.2014.12.019.

[31] E. Fröhlich, The role of surface charge in cellular uptake and cytotoxicity of medical nanoparticles, Int. J. Nanomedicine. 7 (2012) 5577–5591. doi:10.2147/IJN.S36111.

[32] J. Sonnefeld, M. Löbbus, W. Vogelsberger, Determination of electric double layer parameters for spherical silica particles under application of the triple layer model using surface charge density data and results of electrokinetic sonic amplitude measurements, in: Colloids Surfaces A Physicochem. Eng. Asp., Elsevier, 2001: pp. 215–225. doi:10.1016/S0927-7757(01)00845-7.

[33] S. Atalay, Y. Ma, S. Qian, Analytical model for charge properties of silica particles, J. Colloid Interface Sci. 425 (2014) 128–130. doi:10.1016/j.jcis.2014.03.044.

[34] Z. Ovanesyan, A. Aljzmi, M. Almusaynid, A. Khan, E. Valderrama, K.L. Nash, M. Marucho, Ion-ion correlation, solvent excluded volume and pH effects on physicochemical properties of spherical oxide nanoparticles, J. Colloid Interface Sci. 462 (2016) 325–333. doi:10.1016/j.jcis.2015.10.019.

[35] C. Hunley, M. Marucho, Electrical double layer properties of spherical oxide nanoparticles, Phys. Chem. Chem. Phys. 19 (2017) 5396–5404. doi:10.1039/c6cp08174f.

[36] A.N. Filippov, E.Y. Safronova, A.B. Yaroslavtsev, Theoretical and experimental investigation of diffusion permeability of hybrid MF-4SC membranes with silica nanoparticles, J. Membr. Sci. 471 (2014) 110–117. doi:10.1016/j.memsci.2014.08.008.

[37] D.A. Petrova, A.N. Filippov, N.A. Kononenko, S.A. Shkirskaya, M.O. Timchenko, E. V. Ivanov, V.A. Vinokurov, Y.M. Lvov, Perfluorinated hybrid membranes modified by metal decorated clay nanotubes, J. Memb. Sci. 582 (2019) 172–181. doi:10.1016/j.memsci.2019.03.084.

[38] M. Porozhnyy, P. Huguet, M. Cretin, E. Safronova, V. Nikonenko, Mathematical modeling of transport properties of proton-exchange membranes containing immobilized nanoparticles, Int. J. Hydrogen Energy. 41 (2016) 15605–15614. doi:10.1016/j.ijhydene.2016.06.057.

[39] D.J. Belton, O. Deschaume, C.C. Perry, An overview of the fundamentals of the chemistry of silica with relevance to biosilicification and technological advances, FEBS J. 279

(2012) 1710–1720. doi:10.1111/j.1742-4658.2012.08531.x.

[40] A.G. Mikheev, E.Y. Safronova, G.Y. Yurkov, A.B. Yaroslavtsev, Hybrid materials based on MF-4SC perfluorinated sulfo cation-exchange membranes and silica with proton-acceptor properties, Mendeleev Commun. 23 (2013) 66–68. doi:10.1016/j.mencom.2013.03.002.

[41] E.V. Gerasimova, E.Y. Safronova, A.A. Volodin, A.E. Ukshe, Y.A. Dobrovolsky, A.B. Yaroslavtsev, Electrocatalytic properties of the nanostructured electrodes and membranes in hydrogen-air fuel cells, Catal. Today. 193 (2012) 81–86. doi:10.1016/J.CATTOD.2012.06.018.

[42] A. Filippov, D. Afonin, N. Kononenko, Y. Lvov, V. Vinokurov, New approach to characterization of hybrid nanocomposites, Colloids Surfaces A Physicochem. Eng. Asp. 521 (2017) 251–259. doi:10.1016/J.COLSURFA.2016.08.079.

[43] L.T. Zhuravlev, The surface chemistry of amorphous silica, Colloids Surfaces A. 173 (2000) 1. www.elsevier.nl/locate/colsurfa (accessed September 19, 2018).

[44] L. V. Karpenko, O.A. Demina, G.A. Dvorkina, S.B. Parshikov, C. Larchet, B. Auclair, N.P. Berezina, Comparative study of methods used for the determination of electroconductivity of ion-exchange membranes, Russ. J. Electrochem. 37 (2001) 287–293. doi:10.1023/A:1009081431563.

[45] N.D. Pismenskaya, E.E. Nevakshenova, V. V. Nikonenko, Using a Single Set of Structural and Kinetic Parameters of the Microheterogeneous Model to Describe the Sorption and Kinetic Properties of Ion-Exchange Membranes, Pet. Chem. 58 (2018) 465–473. doi:10.1134/S0965544118060087.

[46] E.D. Belashova, N.A. Melnik, N.D. Pismenskaya, K.A. Shevtsova, A. V. Nebavsky, K.A. Lebedev, V. V. Nikonenko, Overlimiting mass transfer through cation-exchange membranes modified by Nafion film and carbon nanotubes, Electrochim. Acta. 59 (2012) 412–423. doi:10.1016/j.electacta.2011.10.077.

[47] J.S. Newman, K.E. Thomas-Alyea, Electrochemical systems, J. Wiley, 2004.

[48] V. Saarinen, K.D. Kreuer, M. Schuster, R. Merkle, J. Maier, On the swelling properties of proton conducting membranes for direct methanol fuel cells, Solid State Ionics. 178 (2007) 533–537. doi:10.1016/j.ssi.2006.12.001.

[49] J. Veerman, D.A. Vermaas, Reverse electrodialysis: Fundamentals, in: Sustain. Energy from Salin. Gradients, Elsevier Inc., 2016: pp. 77–133. doi:10.1016/B978-0-08-100312-1.00004-3.

[50] N.P. Berezina, S. V. Timofeev, N.A. Kononenko, Effect of conditioning techniques of perfluorinated sulphocationic membranes on their hydrophylic and electrotransport

properties, J. Memb. Sci. 209 (2002) 509–518. doi:10.1016/S0376-7388(02)00368-X.

[51] L. Chaabane, G. Bulvestre, C. Larchet, V. Nikonenko, C. Deslouis, H. Takenouti, The influence of absorbed methanol on the swelling and conductivity properties of cation-exchange membranes. Evaluation of nanostructure parameters, J. Membr. Sci. 323 (2008) 167–175. doi:10.1016/j.memsci.2008.06.044.

[52] E.J. Goethals, Telechelic Polymers: Synthesis and Applications., CRC Press, 2017.

[53] R.P. Bagwe, L.R. Hilliard, W. Tan, Surface Modification of Silica Nanoparticles to Reduce Aggregation and Nonspecific Binding, Langmuir. 22 (2006) 4357–4362. doi:10.1021/la052797j.

[54] E. Gerasimova, E. Safronova, A. Ukshe, Y. Dobrovolsky, A. Yaroslavtsev, Electrocatalytic and transport properties of hybrid Nafion® membranes doped with silica and cesium acid salt of phosphotungstic acid in hydrogen fuel cells, Chem. Eng. J. 305 (2016) 121–128. doi:10.1016/J.CEJ.2015.11.079.

[55] N.A. Kononenko, M.A. Fomenko, Y.M. Volfkovich, Structure of perfluorinated membranes investigated by method of standard contact porosimetry., Adv. Colloid Interface Sci. 222 (2015) 425–435. doi:10.1016/j.cis.2014.07.009.

[56] E.Y. Safronova, A.B. Yaroslavtsev, Relationship between properties of hybrid ion-exchange membranes and dopant nature, Solid State Ionics. 251 (2013) 23–27. doi:10.1016/J.SSI.2013.01.011.

[57] V.I. Zabolotsky, V. V. Nikonenko, Effect of structural membrane inhomogeneity on transport properties, J. Membr. Sci. (1993). doi:10.1016/0376-7388(93)85115-D.

[58] N.P. Gnusin, N.P. Berezina, N.A. Kononenko, O.A. Dyomina, Transport structural parameters to characterize ion exchange membranes, J. Membr. Sci. 243 (2004) 301–310. doi:10.1016/J.MEMSCI.2004.06.033.

[59] I. V. Falina, O.A. Demina, N.A. Kononenko, L.A. Annikova, Influence of inert components on the formation of conducting channels in ion-exchange membranes, J. Solid State Electrochem. 21 (2017) 767–775. doi:10.1007/s10008-016-3415-0.

[60] A. Filippov, D. Afonin, N. Kononenko, Y. Lvov, V. Vinokurov, New approach to characterization of hybrid nanocomposites, Colloids Surfaces A Physicochem. Eng. Asp. 521 (2017) 251–259. doi:10.1016/j.colsurfa.2016.08.079.

[61] J. Kamcev, R. Sujanani, E.-S. Jang, N. Yan, N. Moe, D.R. Paul, B.D. Freeman, Salt concentration dependence of ionic conductivity in ion exchange membranes, J. Membr. Sci. 547 (2018) 123–133. doi:10.1016/J.MEMSCI.2017.10.024.

[62] J. Veerman, The Effect of the NaCl Bulk Concentration on the Resistance of Ion Exchange Membranes—Measuring and Modeling, Energies. 13 (2020) 1946.

doi:10.3390/en13081946.

[63] Y. Sedkaoui, A. Szymczyk, H. Lounici, O. Arous, A new lateral method for characterizing the electrical conductivity of ion-exchange membranes, J. Membr. Sci. 507 (2016) 34–42. doi:10.1016/j.memsci.2016.02.003.

[64] В.С. Ничка, С.А. Мареев, М.В. Порожный, С.А. Шкирская, Е.Ю. Сафронова, Н.Д. Письменская, В.В. Никоненко, Модифицированная микрогетерогенная модель для описания электропроводности мембран в разбавленных растворах электролитов, Мембраны и Мембранные Технологии. 9 (2019) 222–232. doi:10.1134/S2218117219030027.

[65] M.T. Bryk, V.I. Zabolotskii, I.D. Atamanenko, G.A. Dvorkina, Structural inhomogeneity of ion-exchange membranes in swelling state and methods of its investigations, J. Water Chem. Technol. 11 (1989) 491–498.

[66] A.B. Yaroslavtsev, Y.A. Karavanova, E.Y. Safronova, Ionic conductivity of hybrid membranes, Pet. Chem. 51 (2011) 473–479. doi:10.1134/S0965544111070140.

[67] K. Oh, O. Kwon, B. Son, D.H. Lee, S. Shanmugam, Nafion-sulfonated silica composite membrane for proton exchange membrane fuel cells under operating low humidity condition, J. Membr. Sci. 583 (2019) 103–109. doi:10.1016/j.memsci.2019.04.031.

[68] F.G. Helfferich, Ionenaustauscher, I, Verlag Chemie, Weinheim, 1959.

[69] B. Auclair, V. Nikonenko, C. Larchet, M. Métayer, L. Dammak, Correlation between transport parameters of ion-exchange membranes, J. Membr. Sci. 195 (2002) 89–102. doi:10.1016/S0376-7388(01)00556-7.

[70] M.A. Andreeva, V. V. Gil, N.D. Pismenskaya, V. V. Nikonenko, L. Dammak, C. Larchet, D. Grande, N.A. Kononenko, Effect of homogenization and hydrophobization of a cation-exchange membrane surface on its scaling in the presence of calcium and magnesium chlorides during electrodialysis, J. Membr. Sci. 540 (2017) 183–191. doi:10.1016/j.memsci.2017.06.030.

[71] B. Zaltzman, I. Rubinstein, Electro-osmotic slip and electroconvective instability, J. Fluid Mech. 579 (2007) 173–226. doi:10.1017/S0022112007004880.

[72] N.A. Mishchuk, Polarization of systems with complex geometry, Curr. Opin. Colloid Interface Sci. 18 (2013) 137–148. doi:10.1016/j.cocis.2013.02.005.

[73] T. Belloň, P. Polezhaev, L. Vobecká, M. Svoboda, Z. Slouka, Experimental observation of phenomena developing on ion-exchange systems during current-voltage curve measurement, J. Membr. Sci. 572 (2019) 607–618. doi:10.1016/j.memsci.2018.11.037.

[74] L. Vobecká, T. Belloň, Z. Slouka, Behavior of Embedded Cation-Exchange Particles in a DC Electric Field, Int. J. Mol. Sci. 20 (2019). doi:10.3390/ijms20143579.

[75] K.A. Nebavskaya, V. V. Sarapulova, K.G. Sabbatovskiy, V.D. Sobolev, N.D. Pismenskaya, P. Sistat, M. Cretin, V. V. Nikonenko, Impact of ion exchange membrane surface charge and hydrophobicity on electroconvection at underlimiting and overlimiting currents, J. Membr. Sci. 523 (2017) 36–44. doi:10.1016/j.memsci.2016.09.038.

[76] H.W. Rösler, F. Maletzki, E. Staude, Ion transfer across electrodialysis membranes in the overlimiting current range: chronopotentiometric studies, J. Membr. Sci. 72 (1992) 171–179. doi:10.1016/0376-7388(92)80197-R.

[77] I. Rubinstein, B. Zaltzman, Equilibrium electroconvective instability, Phys. Rev. Lett. 114 (2015). doi:10.1103/PhysRevLett.114.114502.

[78] S.S. Dukhin, N.A. Mishchuk, Intensification of electrodialysis based on electroosmosis of the second kind, J. Memb. Sci. 79 (1993) 199–210. doi:10.1016/0376-7388(93)85116-E.

[79] I. Rubinstein, B. Zaltzman, Electro-osmotic slip of the second kind and instability in concentration polarization at electrodialysis membranes, Math. Model. Methods Appl. Sci. 11 (2001) 263–300. doi:10.1142/S0218202501000866.

[80] N.A. Mishchuk, The role of water dissociation in concentration polarisation of disperse particles, in: Colloids Surfaces A Physicochem. Eng. Asp., Elsevier Science Publishers B.V., 1999: pp. 467–475. doi:10.1016/S0927-7757(99)00274-5.

[81] P. Sistat, G. Pourcelly, Chronopotentiometric response of an ion-exchange membrane in the underlimiting current-range. Transport phenomena within the diffusion layers, J. Memb. Sci. 123 (1997) 121–131. doi:10.1016/S0376-7388(96)00210-4.

[82] H.J.S. Sand, III. On the concentration at the electrodes in a solution, with special reference to the liberation of hydrogen by electrolysis of a mixture of copper sulphate and sulphuric acid, London, Edinburgh, Dublin Philos. Mag. J. Sci. 1 (1901) 45–79. doi:10.1080/14786440109462590.

[83] R. Simons, Electric field effects on proton transfer between ionizable groups and water in ion exchange membranes, Electrochim. Acta 29 (1984) 151–158. doi:10.1016/0013-4686(84)87040-1.

[84] J.-H. Choi, H.-J. Lee, S.-H. Moon, Effects of Electrolytes on the Transport Phenomena in a Cation-Exchange Membrane, J. Colloid Interface Sci. 238 (2001) 188–195. doi:10.1006/jcis.2001.7510.

[85] M.-S. Kang, Y.-J. Choi, S.-H. Moon, Effects of charge density on water splitting at cation-exchange membrane surface in the over-limiting current region, Korean J. Chem. Eng. 21 (2004) 221–229. doi:10.1007/BF02705402.

[86] S. Zyryanova, S. Mareev, V. Gil, E. Korzhova, N. Pismenskaya, V. Sarapulova, O. Rybalkina, E. Boyko, C. Larchet, L. Dammak, V. Nikonenko, How Electrical

Heterogeneity Parameters of Ion-Exchange Membrane Surface Affect the Mass Transfer and Water Splitting Rate in Electrodialysis, Int. J. Mol. Sci. 21 (2020) 973. doi:10.3390/ijms21030973.

[87] V.I. Zabolotskiy, A.Y. But, V.I. Vasil'eva, E.M. Akberova, S.S. Melnikov, Ion transport and electrochemical stability of strongly basic anion-exchange membranes under high current electrodialysis conditions, J. Membr. Sci. 526 (2017) 60–72. doi:10.1016/j.memsci.2016.12.028.

[88] Z. Slouka, S. Senapati, Y. Yan, H.C. Chang, Charge inversion, water splitting, and vortex suppression due to DNA sorption on ion-selective membranes and their ion-current signatures, Langmuir. 29 (2013) 8275–8283. doi:10.1021/la4007179.

[89] T. Belloň, Z. Slouka, Overlimiting behavior of surface-modified heterogeneous anion-exchange membranes, J. Membr. Sci. 610 (2020) 118291. doi:10.1016/j.memsci.2020.118291.

[90] S.A. Mareev, E. Evdochenko, M. Wessling, O.A. Kozaderova, S.I. Niftaliev, N.D. Pismenskaya, V. V. Nikonenko, A comprehensive mathematical model of water splitting in bipolar membranes: Impact of the spatial distribution of fixed charges and catalyst at bipolar junction, J. Membr. Sci. 603 (2020) 118010. doi:10.1016/j.memsci.2020.118010.

[91] S. Mafé, P. Ramírez, A. Alcaraz, Electric field-assisted proton transfer and water dissociation at the junction of a fixed-charge bipolar membrane, Chem. Phys. Lett. 294 (1998) 406–412. doi:10.1016/S0009-2614(98)00877-X.

[92] H. Strathmann, J.. Krol, H.-J. Rapp, G. Eigenberger, Limiting current density and water dissociation in bipolar membranes, J. Membr. Sci. 125 (1997) 123–142. doi:10.1016/S0376-7388(96)00185-8.

[93] Z. Yan, L. Zhu, Y.C. Li, R.J. Wycisk, P.N. Pintauro, M.A. Hickner, T.E. Mallouk, The balance of electric field and interfacial catalysis in promoting water dissociation in bipolar membranes, Energy Environ. Sci. 11 (2018) 2235–2245. doi:10.1039/C8EE01192C.

[94] R. Simons, Electric field effects on proton transfer between ionizable groups and water in ion exchange membranes, Electrochim. Acta 29 (1984) 151–158. doi:10.1016/0013-4686(84)87040-1.

[95] M. Barisik, S. Atalay, A. Beskok, S. Qian, Size Dependent Surface Charge Properties of Silica Nanoparticles, J. Phys. Chem. C. 118 (2014) 1836–1842. doi:10.1021/jp410536n.

[96] L.T. Zhuravlev, Concentration of Hydroxyl Groups on the Surface of Amorphous Silicas, Langmuir. 3 (1987) 316–318. doi:10.1021/la00075a004.

[97] L.T. Zhuravlev, Surface characterization of amorphous silica-a review of work from the former USSR, Colloids Surfaces A Physicochem. Eng. Asp. 74 (1993) 71–90.

doi:10.1016/0927-7757(93)80399-Y.

[98] D.R. Lide, Handbook of Chemistry and Physics, CRC Press: New York, NY, USA, 1995.

[99] M. Anastassiades, E. Scherbaum, Chapter 4. Sample handling and clean-up procedures II-new developments, 2005. doi:10.1016/S0166-526X(05)80024-8.